Materials Science & Engineering A 844 (2022) 143196

Contents lists available at ScienceDirect

Materials Science & Engineering A

journal homepage: www.elsevier.com/locate/msea

Laser additive manufacturing of Inconel 718 at increased deposition rates

Chongliang Zhong [a,*], Andres Gasser [a], Gerhard Backes [b], Jinbao Fu [c], Johannes Henrich Schleifenbaum [b]

[a] Fraunhofer ILT - Institute for Laser Technology, Aachen, Germany
[b] RWTH Aachen University DAP - Digital Additive Production, Aachen, Germany
[c] Changchun Institute of Optics, Fine Mechanics and Physics, Chinese Academy of Sciences, Changchun, China

ARTICLE INFO

Keywords:
Laser additive manufacturing
Direct energy deposition
Inconel 718
Deposition rate
Mechanical properties

ABSTRACT

Inconel 718 (IN718) is a nickel-based superalloy designed to display exceptionally high yield, tensile and creep-rupture properties at temperatures up to approx. 700 °C. For aerospace applications, it is the most widely used superalloy. The additive manufacturing process, laser-based direct energy deposition (DED) with powdery filler material can be used to repair, geometrically modify or manufacture components made of IN718. However, despite the devious advantages, its typical deposition rate of <0.5 kg/h is significantly lower than that of other DED processes such as metal inert gas (MIG) of wire + arc additive manufacturing (WAAM) – at about 10 kg/h – and electron beam additive manufacturing (EBAM®) with wire - at approx. 12 kg/h. Here, using IN718 as additive material, we targeted to increase the deposition rate of laser-based DED by a factor of more than ten and achieved a deposition rate of about 6 kg/h. For this purpose, we first developed a suitable process management strategy in combination with adapted system technology. Then, we built up samples with developed process parameters, from which tensile specimens for mechanical property tests were manufactured. Thereafter, the macro- and microstructures of the as-deposited material were analyzed. Based on the results, we applied a post heat treatment for modifying the microstructure and improving the mechanical properties. We demonstrated finally, the aerospace material specifications for the static mechanical properties can be achieved. This work shows a great potential of laser-based DED with increased deposition rate.

1. Introduction

For metallic materials, laser-based direct energy deposition (DED) with powdery filler material is one of the most important additive manufacturing (AM) processes. Compared to powder bed based processes, such as EPBF (electron powder bed fusion) or LPBF (laser powder bed fusion), the main advantages of this process are its broad applicability for cladding, repair and, increasingly, additive manufacturing, as well as its ability both to process large components (in the meter range) and to modify conventionally manufactured components, for example, by deposition or manufacturing geometric features. Laser-based DED with powdery filler material is currently used, particularly, in turbomachinery and aerospace industries to process high performance materials such as nickel-based superalloys.

The superalloy Inconel 718 (IN718) is such a nickel-based alloy and typically used for manufacturing high temperature turbine components. The reason for this is its good mechanical properties, such as high wear resistance, tensile strength and creep resistance at temperatures up to 700 °C. In the area of additive manufacturing, many research has been done regarding the material properties of IN718, and AM of IN718 is more and more widely applied for a variety of applications [1,2]. Components made of IN718 can be processed with the laser-based DED as described above. When appropriate post heat treatment is applied, the aerospace material specifications (AMS) for the static mechanical properties can be achieved and are similar to that of wrought material [3].

To date, a deposition rate of less than 0.5 kg/h can be achieved by laser-based DED to process IN718 with coaxial powder feeding and without additional energy sources such as induction heating for preheating [4]. However, this is very low compared to the deposition rates of other DED processes such as metal inert gas (MIG) of wire + arc additive manufacturing (WAAM), which reaches about 10 kg/h [5–7], and electron beam additive manufacturing (EBAM®) with wire, which achieves up to approx. 12 kg/h [8]. Nevertheless, the scope of the

* Corresponding author.
E-mail address: chongliang.zhong@gmail.com (C. Zhong).

https://doi.org/10.1016/j.msea.2022.143196
Received 15 May 2021; Received in revised form 20 March 2022; Accepted 21 April 2022
Available online 25 April 2022

applications with laser-based DED is continuously increasing. This process is also becoming more and more attractive for additive manufacturing, especially in combination with conventional manufacturing processes. For these reasons, there is a growing demand to increase the deposition rate significantly and, thus, to improve the productivity of the process. The main goal of the work presented here was to increase the deposition rate by at least a factor of 10, to more than 5 kg/h, and at the same time, to achieve the aerospace material specifications (AMS) for the static mechanical properties.

To achieve these targets, we initially developed a suitable process management strategy in combination with adapted system technology, especially the powder feeding nozzle, for the mentioned deposition rates. Then, we built cuboids with developed process parameters, from which tensile specimens for mechanical property tests were manufactured. Thereafter, the macro- and microstructures of the as-deposited material were analyzed. Based on the results, a post heat treatment was adapted and conducted in order to modify the microstructure. To investigate the effects of this heat treatment, we then analyzed the microstructure of the heat-treated material. Finally, the static mechanical properties were determined through tensile tests. These properties were compared with the AMS specifications to evaluate the achieved results.

2. Method

When it is assumed that the cross section of a single track is a half ellipse, the functional dependency of the deposition rate on the process parameters can be expressed by

$$\dot{m}_{Ar} = A_S \cdot v \cdot \rho \approx \frac{1}{2} \cdot \pi \cdot \frac{d_L}{2} \cdot h_B \cdot v \cdot \rho = \frac{1}{4} \cdot \pi \cdot B_v \cdot {d_L}^2 \cdot v \cdot \rho \quad (1)$$

where.

$\dot{m}_{Ar}$: Deposition rate.
A_S: Cross-sectional area of a single track.
v: Scanning speed.
ρ: Density of the material.
d_L: Diameter of the laser spot.
h_B: Layer thickness.
b: Layer width, $b \approx d_L$ and.
B_v: Aspect ratio, $B_v = h_B/b \approx h_B/d_L$.

According to Equation (1), the deposition rate is proportional to the scanning speed and to the square of the laser spot diameter with a constant aspect ratio. The deposition rate can thus be increased by increasing either the scanning speed or the laser spot diameter. Since the laser spot diameter influences the deposition rate more significantly, the laser spot diameter is enlarged, and laser power increased. To accomplish this approach, an experimental setup was built up, see Fig. 1.

The typical laser spot diameter used in DED lies in the range of 0.5–1.5 mm, with which the system can achieve a deposition rate of up to about 0.5 kg/h. By using a laser spot diameter of approx. 4 mm, Zhong [4,9] and Witzel [10] have demonstrated that deposition rates of up to about 2 kg/h can be achieved. Here, a zoom optic was used to generate a larger laser spot, up to ∅ 9 mm in the working plane. Since a sufficient laser power is the key prerequisite for increasing the deposition rate, a

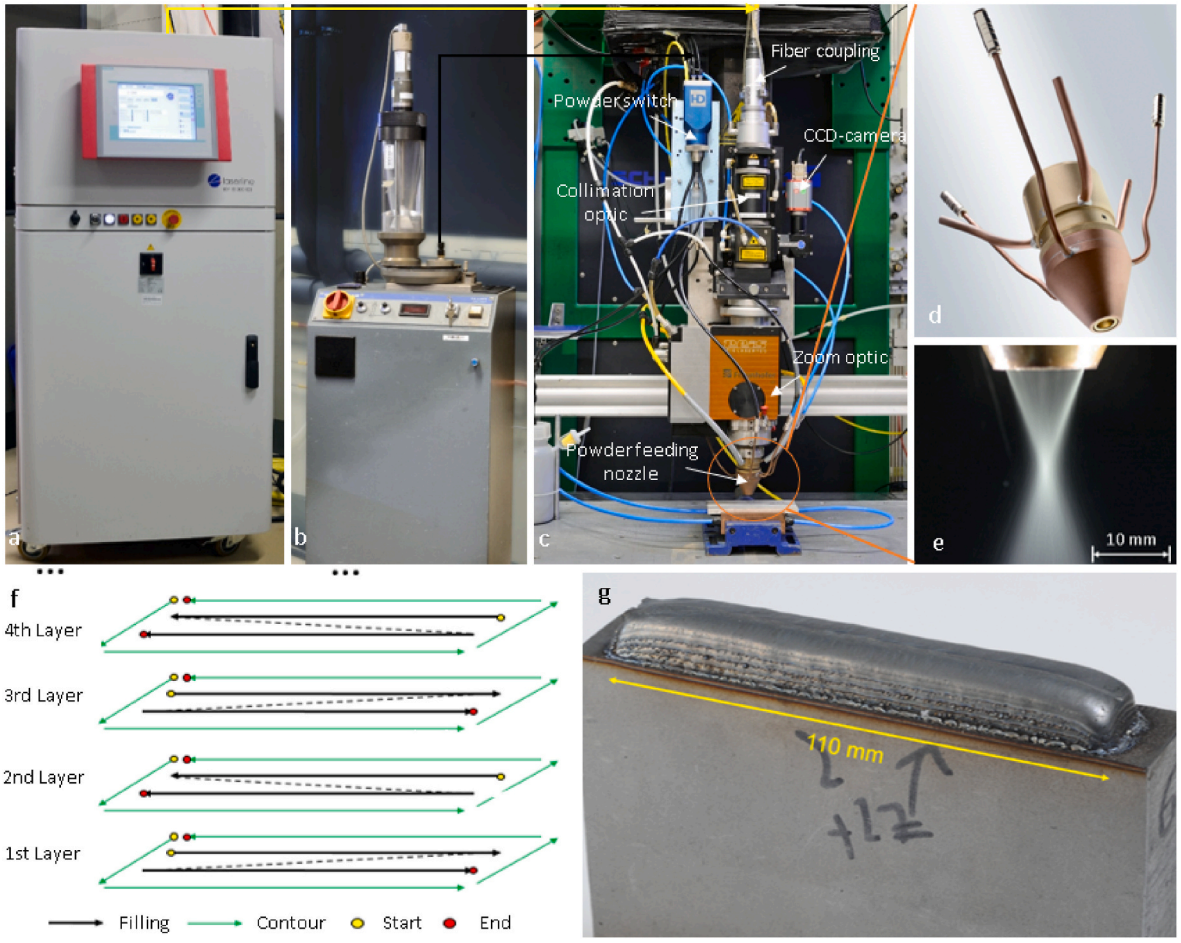

Fig. 1. | Experimental setup: a The high power laser source, a diode laser with a max. output of 12 kW; **b** The powder feeder; **c** The main experimental setup; **d** The powder feeding nozzle; **e** The powder-gas-flow with a powder flow rate of approx. 7 kg/h, where a homogenous powder distribution can be observed. **f** The deposition strategy: the layers are deposited in a meandering pattern, and for every layer, a contour is deposited. **g** A deposited cuboid.

high power diode laser with a maximum output power of approx. 12 kW was used in this work.

Another challenge for implementing laser-based DED with high deposition rates is the powder feeding nozzle, which has two essential requirements in comparison to conventional DED. First, the nozzle must be resistant to high thermal loads because it is exposed to a significantly high heat radiation and reflections from the higher laser power. Second, to achieve a deposition rate of more than 5 kg/h, a powder flow rate higher than 5 kg/h must be fed through the nozzle without creating a stoppage in it. To achieve these targets, a modified powder feeding nozzle, based on the ILT-KOAX-50 nozzle, was used for this work.

As shown in Fig. 1, the laser beam generated by the laser source is guided via a fiber through the processing optic to the workpiece. The additive material that fed by a powder feeder comes through the powder tubes and the powder switch and then is injected via the powder feeding nozzle into the laser-induced molten pool. The powder tubes are electrically conductive so that electrostatic charges are avoided. The process can be observed coaxially via the integrated CCD camera on the connected monitor.

The whole experimental setup mainly consists of a high power laser source with a maximal output powder of approx. 12 kW, a collimator, a zoom optic and a modified powder feeding nozzle for processing high powder flow rates up to >7 kg/h. The setup is equipped with a four-axis handling system. Both the tool axis and the movement of the lenses in the zoom optic are controlled by a NC-control system. With the zoom optic, the size of the circular laser spot can be varied from a diameter of 3 mm–9 mm. The 12 kW diode laser source is linked via a 1000 μm glass fiber to the collimation optic. The powder is fed by argon, which is also used as the shielding gas, preventing the molten pool from interacting with atmospheric gases such as O_2.

3. Process development

3.1. Materials

For the study, powders manufactured with two different processes were used: gas atomization (GA) and plasma rotating electrode process (PREP). Both powders have the same nominal grain size in the range of 45–90 μm. The chemical compositions of the powders used are listed in Table 1. In addition, to evaluate these values, the limit values regarding the chemical composition of IN718 [11] are given as well in this table.

As seen in Table 1, both powders have a quite similar chemical composition and satisfy the specifications.

The morphology of the powders was analyzed with a light microscope (LM) and scanning electron microscope (SEM), see Fig. 2.

As is common for powder manufactured by the GA process, a certain amount of powder particles shows small adherences, so-called satellites. These satellites are formed during the gas atomization process: Smaller rapidly solidified particles adhere to the larger and semi-liquid particles. Moreover, non-uniform and non-spherical particles can be observed. Additionally, hollow particles with pores inside the particles can be also observed from the polished cross-sections in the LM micrographs.

In comparison to the GA powder, very few irregular-shaped or non-uniform particles can be found in the powder manufactured by the PREP process. The particles are almost perfectly spherical and have neither enclosed pores nor adhering satellites. To sum up, PREP powder shows a better quality than GA powder. Nevertheless, PREP powder is much more expensive, and owing to this GA powder was initially used in the process development to identify the process parameters in the next step.

3.2. Initial process parameters and procedure

The target was to identify the process parameters by doing experiments and conducting evaluations. The following procedure was applied to find suitable initial parameters.

The deposition rate is dependent upon the process parameters: According to Equation (1), the deposition rate is proportional to both the scanning speed and the square of the laser spot diameter with a constant aspect ratio.

Laser spot diameter: Since the laser spot diameter has the greatest influence on the deposition rate, the maximum laser spot that can be achieved with the optical system, φ 9 mm, was used.

Powder flow rate: In order to achieve a deposition rate of 5 kg/h, a powder flow rate of approximately 5.6 kg/h is necessary, assuming a powder efficiency of 90%. Since a deposition rate of >5 kg/h should be achieved, a powder flow rate of about 6 kg/h was determined.

Scanning speed: With an aspect ratio of approx. 1:5, a density for IN 718 of approx. 8.2 g/cm^3, a deposition rate of 5 kg/h, and a scanning speed of 799 mm/min are calculated with equation (1) above. As starting value, a scanning speed of 800 mm/min was selected.

Laser power: The laser power was the last parameter to be determined. According to Witzel [10], the laser power required tends to increase only disproportionately with increasing powder flow rate. It is, thus, difficult to estimate the necessary laser power through the powder flow rate. Nevertheless, preliminary tests show that a laser power of approx. 5.6 kW is required to prevent bonding defects and guarantee a metallurgical bonding. In order to determine a suitable laser power, experiments with variation of the laser power in the range 5.6–7.5 kW were, therefore, conducted.

Three groups of experiments (Table 2) were conducted to examine the influence of the process parameters on porosity and track geometry. The laser spot diameter remains constant for all experiments and is approx. 9 mm. Single tracks of about 80 mm in length are deposited, metallographically prepared and evaluated. For the evaluations, three positions of each deposited track far from the start and end positions were analyzed.

3.3. Effect of laser power

As discussed above, the laser power cannot be determined by the afore-mentioned equation. Thus, for the experiments, the laser power was first varied in the range of 5.6–7.5 kW. The effects of laser power on porosity and track geometry (track width, track thickness and aspect ratio) are presented in Fig. 3.

As shown, the porosity decreases as laser power increases, from almost 3.2% at approx. 5.6 kW to 0.27% at approx. 7.5 kW. At a laser power of approx. 6.6 kW, the single tracks have a significantly lower porosity. It is also striking that the fluctuations in the porosity are significantly greater at lower laser powers than at high laser powers. Nevertheless, a completely dense single track could not be achieved even at a laser power of approx.7.5 kW.

Regarding the track geometry, the single tracks become wider with increasing laser power. The change in the track thickness as the laser power increases is not significant. These changes in the track geometry lead to a slight decrease in the aspect ratio, from approx. 0.2 to 0.17.

As a laser power of 6.6 kW is sufficient to achieve the lowest porosity

Table 1
The chemical composition of the powders used.

		Ni	Cr	Nb	Mo	Ti	Al	Mn	C	S
Specification		50.0–55.0	17.0–21.0	4.75–5.50	2.80–3.30	0.65–1.15	0.20–0.80	<0.35	<0.08	<0.015
Powder	GA	53,07	18.48	4.86	3.01	0.92	0.33	0.18	0.026	0.002
	PREP	51.3	19.2	5.2	3.0	0.99	0.56	0.037	0.056	0.004

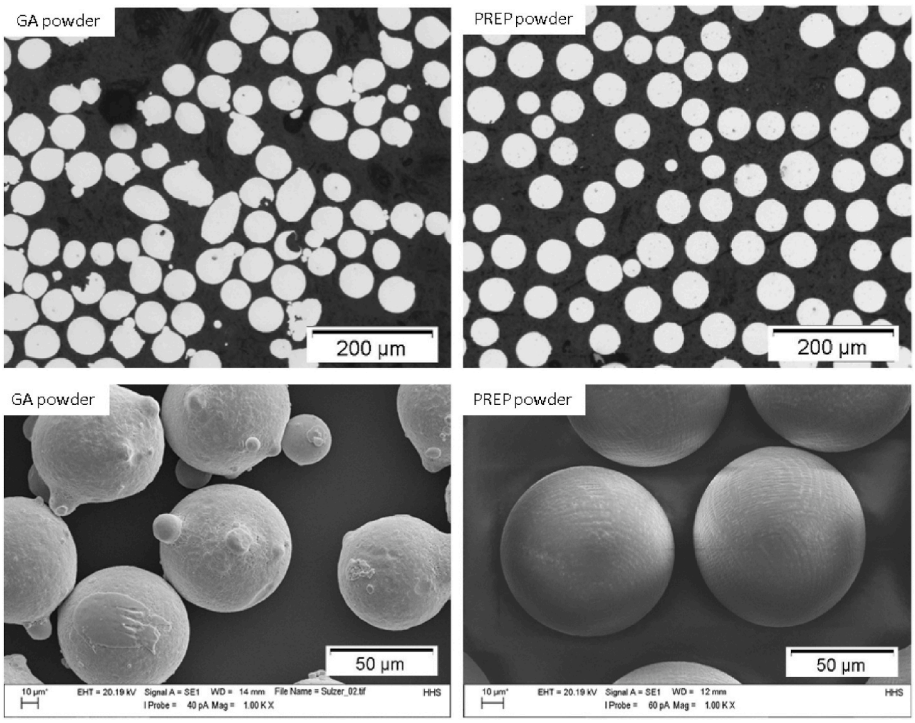

Fig. 2. Light microscope (LM) and scanning electron microscope (SEM) micrographs of the powders used.

Table 2
Experimental plan for studying the effects of the main process parameters.

	Laser power P_L [kW]	Scanning speed v [mm/min]	Powder flow rate $\dot{m}$ [kg/h]
Group 1	5.6–7.5	800	6
Group 2	6.6	600–1000	6
Group 3	6.6	800	5–7

of 0.27%, this laser power was used for the further experiments.

3.4. Effect of scanning speed

In the following experiments, the feed speed was varied in the range of 600–1000 mm/min, at constant laser power and power flow rate.

As shown in Fig. 4, the porosity remains almost constant up to a scanning speed of approx. 900 mm/min and then increases sharply. Both the track thickness and the track width decrease slightly with increasing scanning speed. Since the track thickness decreases faster than the track width, the aspect ratio decreases slightly as the scanning speed increases. By applying the estimated scanning speed of 800 mm/min, low porosity could be achieved and no negative effects on the track geometry are observed; therefore, this value was retained for the further experiments.

3.5. Effect of powder flow rate

For the following experiments, the powder flow rate was varied in the range of approx. 5–7 kg/h.

As can be seen in Fig. 5, the porosity initially remains constant as the powder flow rate increases, then increases significantly. It is also easy to recognize that the fluctuation of the porosity increases as powder flow rate increases, from about 6 kg/h. At a powder flow rate <6 kg/h, the porosity is approx. 0.3%.

Regarding the track geometry, the single tracks become slightly higher as the powder flow rate increases, whereas the track width remains almost constant. The aspect ratio increases from 0.15 to 0.21.

3.6. Process parameters

According to Witzel [10], a porosity smaller than 0.25% is required for aerospace applications. However, a porosity of lower than 0.25%

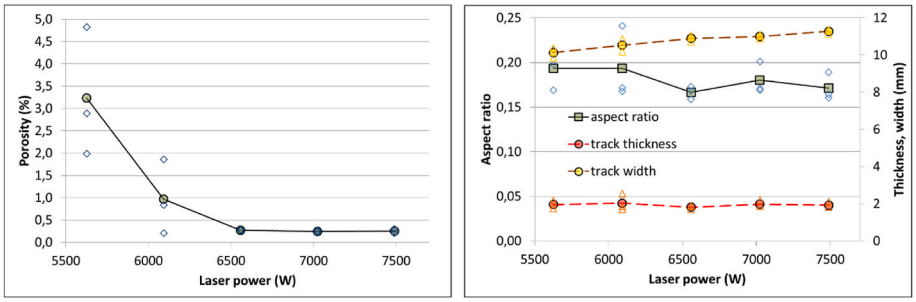

Fig. 3. The influence of laser power on porosity (left) and track geometry (right). The powder flow rate of approx. 6 kg/h and the scanning speed of 800 mm/min remain constant.

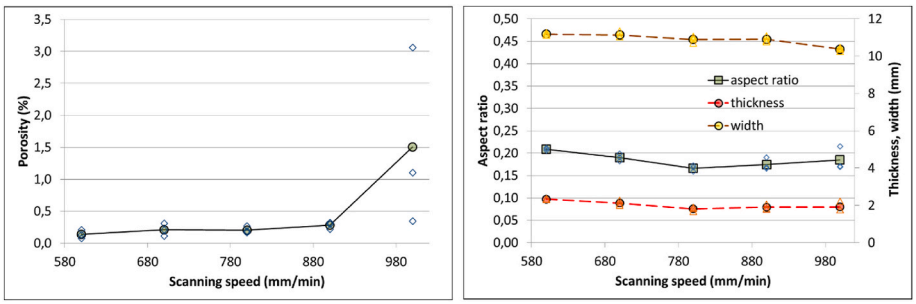

Fig. 4. The influence of scanning speed on porosity (left) and track geometry (right). The laser power of approx.6.6 kW and the powder flow rate of approx. 6 kg/h remain constant.

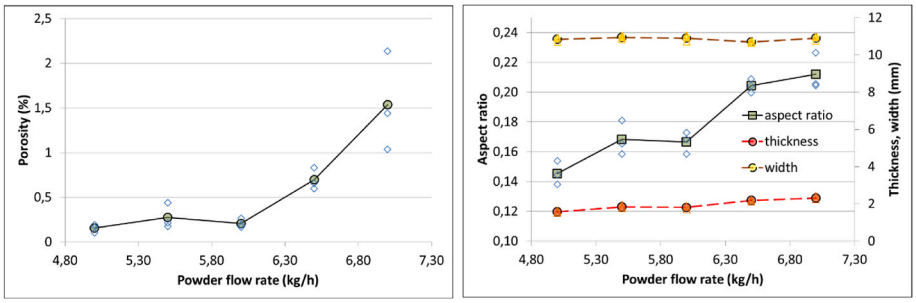

Fig. 5. The influence of powder flow rate on porosity (left) and track geometry (right). The feed rate of 800 mm/min and the laser power of approx.6.6 kW remain constant.

cannot be achieved with the GA powder. Zhong et al. have shown that the porosity can be essentially decreased by using PREP powder [12]. Therefore, PREP powder was used for the further experiments.

For the parameter transmission, we observe that more particles are "reflected" from the melt in the process with PREP powder. The reason is presumably the higher particle speed of the PREP particles due to their morphology: They have a much smoother surface than GA-powder and the particles are nearly perfectly spherical. In order to achieve a similar deposition rate, the powder flow rate, therefore, had to be increased by approx. 4–5%. The basic parameters for both powders and typical cross sections of the deposited single tracks are depicted in Fig. 6.

With a laser spot diameter of approx. 9 mm, this experimental setup could achieve a deposition rate of around 6 kg/h at a laser power of approx. 6.6 kW, a powder flow rate of about 6.5 kg/h and a scanning speed of 800 mm/min. Based on these basic process parameters, 3D geometries such as cuboids, shown in Fig. 1, were built up using PREP powder. Since the workpiece was continuously heated during the process, the laser power was successively adapted to avoid excessive heat input and, thus, to prevent the melt from overheating, which is intended to reduce or avoid deformation. To adapting the laser power, the Z-traverse distance needs to stay constant for each layer so that the layer thickness remains as unchanged as possible. The parameters used for the cuboid are listed in Table 3.

From the cuboids, tensile test specimens were manufactured according to DIN 50125-B 4x20 for studying the static mechanical properties.

4. Microstructure and mechanical properties

4.1. Macro- and microstructure

The macro- and microstructure of the as-deposited material were analyzed by using a light microscope (LM) and a scanning electron microscope (SEM). Regarding the macrostructure, the tensile specimen is free of cracks and exhibits a very low porosity, see Fig. 7. To study the microstructure, the as-deposited material is etched, after which columnar grains mainly aligned perpendicular to the deposition direction can be observed, thus indicating a strong anisotropy. Moreover, the

Table 3
Process parameters for building up the cuboid with PREP powder.

Layer	Track	Laser power P_L [kW]	Scanning speed v [mm/min]	Power flow rate $\dot{m}$ [kg/h]
1	1	6.6	800	6.5
	2	6.4	800	6.5
2–5	1	6.4	800	6.5
	2	6.2	800	6.5

	GA powder	PREP powder
Laser power [kW]	6.6	6.6
Scanning speed [mm/min]	800	800
Powder flow rate [kg/h]	6.3	6.5

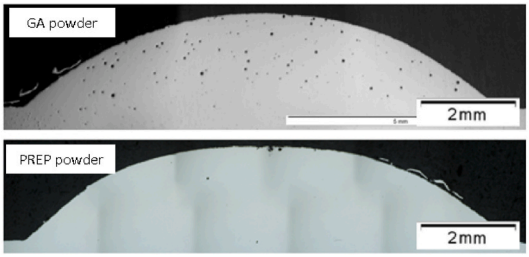

Fig. 6. The basis process parameters (left) and typical cross sections by applying these process parameters (right).

dendritic structure can be observed, and there is a large amount of Laves phases in the interdendritic zones. The microstructure is presented in Fig. 7.

It is worth mentioning here that the Laves phase is an intermetallic and long-chained brittle phase in IN718 [13,14], which is detrimental for the mechanical properties, such as ductility, ultimate tensile strength, fracture toughness and fatigue life [15–17]. Moreover, IN718 is strengthened primarily by the body-centered tetragonal (BCT) γ''-phases (Ni_3Nb) and, to a small extent, by the face-centered cubic (FCC) γ'-phases ($Ni_3(Al,Ti)$) [18,19]. However, none of these strengthening phases were observed in the as-deposited material. These overserved microstructures, columnar grains, the dendritic structure and the Laves phases are very similar to the typical microstructures of the as-deposited IN718 in conventional DED [20–22].

In summary, though no obvious defects and a very low porosity were achieved, the as-deposited material shows a strong anisotropy. Additionally, there is a high amount of detrimental Laves phases, while strengthening phases are not available, which indicates poor mechanical properties. In order to improve the microstructure and, thus, mechanical properties, a post heat treatment must be applied.

4.2. Heat treatment

According to the problems identified in the as-deposited material, the following targets should be achieved by a post heat treatment: elimination of the anisotropy, dissolving of the Laves phases, and precipitation of the strengthening phases. Therefore, a three-step heat treatment consisting of homogenization, solution and double aging was applied.

To eliminate the anisotropy, the as-deposited material was firstly homogenized for 2 h at a temperature of approx. 1100 °C, and then cooled down in air. Through homogenization, all the alloy elements should be homogeneously distributed in the matrix, which can eliminate the anisotropy and dissolve the Laves phases [10]. Afterwards, the samples were solution heat treated for another 2 h at a temperature of about 980 °C, and then cooled down in air. Through this step, δ-phases can be formed and are located at the grain boundaries. δ-phases are important for the further heat treatment because they prevent the grain growth [23] and, therefore, hinder the grain coarsening that is detrimental to the static mechanical properties. Finally, the as-deposited materials were double aged: at approx. 720 °C for 10 h, cooled down in an oven to 620 °C, and then aged for another 20 h under 620 °C. Through double-aging, the strengthening phases should be precipitated, thus improving the mechanical properties.

In order to prove whether the targets of the heat treatment were achieved, the microstructure of the heat treated material was analyzed using light microscope (LM), (scanning electron microscope) SEM and electron backscatter diffraction (EBSD). The grain morphology, grain orientation and the precipitations were observed and the results are presented in Fig. 8.

After the heat treatment, the columnar grains were transformed to equiaxed grains, which can be seen in the LM micrographs and the results of the EBSD analysis. The isotropic orientations of the grains can be seen in the EBSD-IPF map. AS well, the pole figures show very similar patterns. All this indicates that the anisotropy of the as-deposited material is eliminated through the applied heat treatment. In the heat-treated material, no Laves phase is observed, which suggests they have been successfully dissolved. Moreover, the needle-like δ-phases are observed at the grain boundaries. Their morphology and location indicate that grain growth during the heat treatment can be avoided. Furthermore, the strengthening phases are precipitated in the matrix, which improve the strength of the material. In summary, all the aforementioned targets were achieved by the applied three-step post heat treatment. Since the material exhibits no cracking and has a low porosity, and the desired microstructures are obtained after heat treatment, the expected mechanical properties should be achieved.

4.3. Mechanical properties

To determine the static mechanical properties, tensile tests were carried out. The ultimate strength, the yield strength and the elongation were determined, and the results are presented in Fig. 9. In order to evaluate these achieved results, the specifications according to AMS (Aerospace Material Specification) for cast IN718 (AMS 5383) and wrought IN718 (AMS 5662) are also presented in Fig. 9.

It can be seen in Fig. 9 that all the achieved static mechanical properties satisfy both of the specifications: The achieved properties are significantly higher than those of cast IN718 and are quite similar to those of wrought IN718.

5. Summary

In summary, we have demonstrated that the deposition rate of laser-based DED with IN718 can be increased by a factor of more than ten – from lower than 0.5 kg/h (state of the art) to more than 5 kg/h and up to approx. 6 kg/h – by enlarging the laser spot diameter and raising the laser power along with using the corresponding system technology, especially the powder feeding nozzle.

1. We achieved quite similar microstructures to that of the as-deposited material in conventional laser-based DED with IN718: columnar grains with dendritic structure, a large amount of Laves phases located at the interdendritic zones, and no available strengthening phases.
2. To improve the microstructure and, thus, the mechanical properties, the as-deposited material was heat treated by homogenization, solution and double aging.
3. After heat treatment, the anisotropy is eliminated, the Laves phases are dissolved and the strengthening phases precipitated.

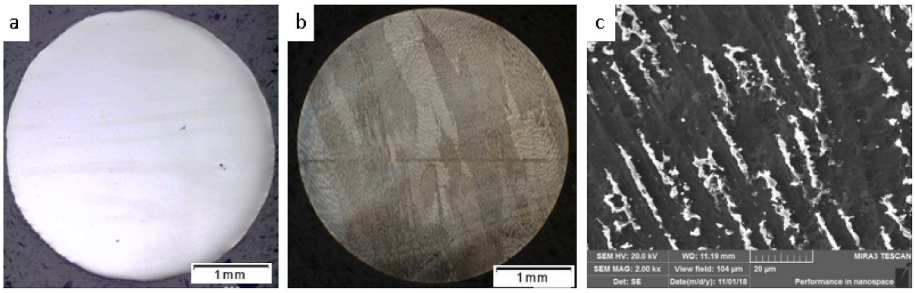

Fig. 7. | Macro- and microstructure of the as-deposited material: a A light microscope (LM) micrograph of a polished cross section showing the nearly defect-free as-deposited material; **b** An LM micrograph of an etched cross-section, where the columnar grains and the dendritic structure can be seen. **c** A scanning electron microscope (SEM) micrograph, showing the detail of the dendritic structure and the Laves phases (the bright white phases) which are in the interdendritic areas.

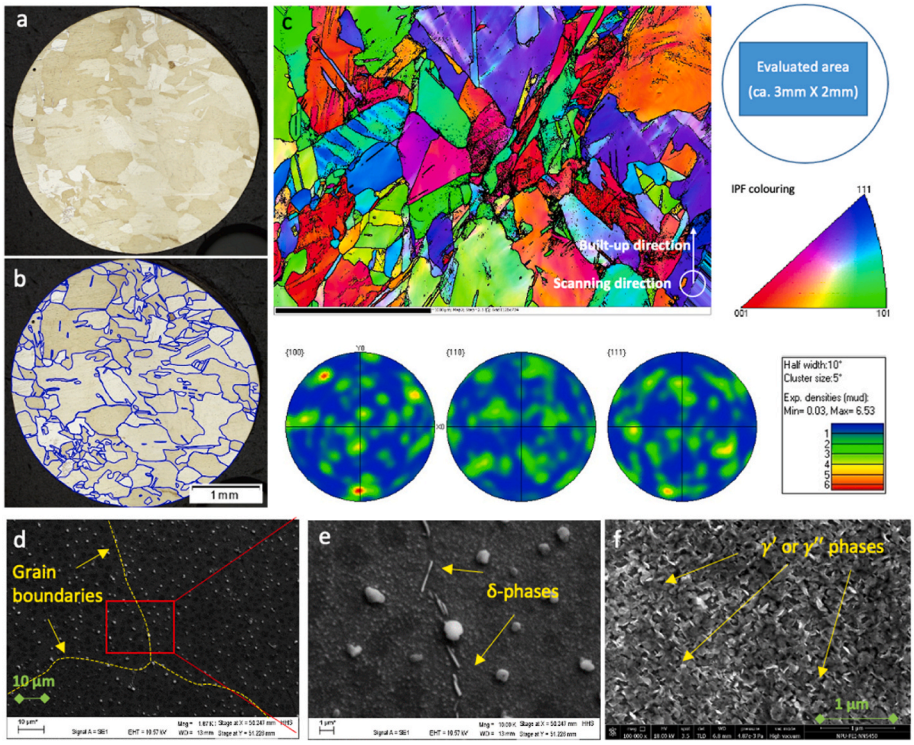

Fig. 8. | The microstructure of the heat treated material: a An LM micrograph of an etched cross-section of the heat-treated material. Instead of columnar grains, equiaxed grains can be observed. **b** The grain boundaries are marked with blue, by which the morphology of the grains can be clearly recognized. **c** The results of electron backscatter diffraction (EBSD) analysis, the heat treated material can be seen as nearly isotropic. **d** A SEM micrograph showing the grain boundaries (marked with yellow). The area in the box is observed at a higher magnification with SEM and is shown in **e,** where δ-phases located at the grain boundaries can be seen. **f** An SEM micrograph showing the even distribution of the strengthening phases. (For interpretation of the references to colour in this figure legend, the reader is referred to the Web version of this article.)

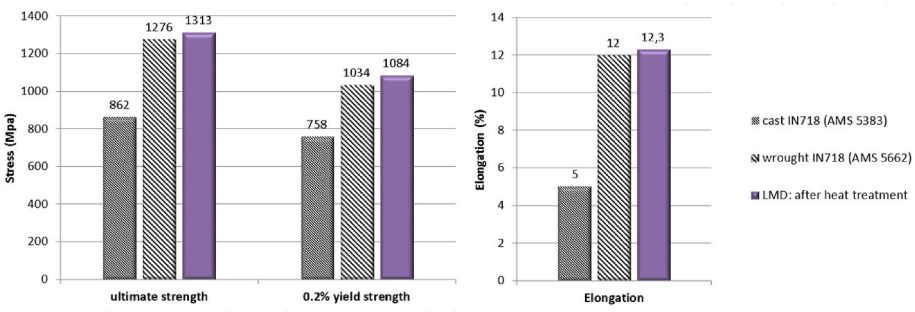

Fig. 9. | Static mechanical properties: The achieved ultimate strength, yield strength and elongation in this work are presented in violet columns. To help evaluate the results, the AMS (Aerospace Material Specification) for cast and wrought IN718 are also given. The achieved static mechanical properties are significantly higher than the specifications for cast IN718 and are similar to those of wrought material. (For interpretation of the references to colour in this figure legend, the reader is referred to the Web version of this article.)

4. The static mechanical properties were determined through tensile tests. The results show that the ultimate strength, the yield strength and the elongation satisfy the AMS specifications.

The material exhibits significant better performance than the cast material and is very similar to that of wrought IN718. Last but not least, the methodology for increasing the deposition rate is not limited in IN718, but can be applied as well to other materials that can be additively manufactured by laser-based DED.

CRediT authorship contribution statement

Chongliang Zhong: Conceptualization, Methodology, Investigation, Validation, Formal analysis, Writing – original draft, Writing – review & editing, Visualization, Project administration. **Andres Gasser:** Conceptualization, Methodology, Supervision. **Gerhard Backes:** Conceptualization, Methodology, Investigation, Validation, Formal analysis. **Jinbao Fu:** Conceptualization, Methodology, Writing – review & editing.

Declaration of competing interest

The authors declare that they have no known competing financial interests or personal relationships that could have appeared to influence the work reported in this paper.

Acknowledgments

This research was supported by Chinesisch-Deutsches Zentrum für Wissenschaftsförderung [GZ 1267] and Deutsche Forschungsgemeinschaft [GZ: GA 2411/1-1].

The raw/processed data required to reproduce these findings cannot be shared at this time as the data also forms part of an ongoing study.

References

[1] L. Ladani, Additive Manufacturing of Metals: Materials, Processes, Tests, and Standards, DEStech Publications, Incorporated, 2021.
[2] Magda Sadowski, et al., Optimizing quality of additively manufactured Inconel 718 using powder bed laser melting process, Addit. Manuf. 11 (2016) 60–70.
[3] X. Zhao, J. Chen, X. Lin, W. Huang, Study on microstructure and mechanical properties of laser rapid forming Inconel 718, Mater. Sci. Eng., A 478 (2008) 119–124.
[4] C. Zhong, A. Gasser, J. Kittel, K. Wissenbach, R. Poprawe, Improvement of material performance of Inconel 718 formed by high deposition-rate laser metal deposition, Mater. Des. 98 (2016) 128–134.
[5] D. Ding, Z. Pan, S. van Duin, H. Li, C. Shen, Fabricating superior NiAl bronze components through wire arc additive manufacturing, Materials 9 (2016) 652.

[6] F. Martina, et al., Tandem metal inert gas process for high productivity wire arc additive manufacturing in stainless steel, Addit. Manuf. 25 (2019) 545–550.
[7] T.A. Rodrigues, V. Duarte, R.M. Miranda, T.G. Santos, J.P. Oliveira, Current status and perspectives on wire and arc additive manufacturing (WAAM), Materials 12 (2019) 1121.
[8] Sciaky Inc, Benefits of Wire vs. Powder Metal 3D Printing. Comparing Sciaky's wirefeed 3D printing process, a.k.a. Electron Beam Additive Manufacturing, to powder-based feedstock 3D printing processes, Available at: https://www.sciaky.com/additive-manufacturing/wire-vs-powder.
[9] C. Zhong, et al., Microstructures and tensile properties of Inconel 718 formed by high deposition-rate laser metal deposition, J. Laser Appl. 28 (2016) 22010.
[10] J. Witzel, Universitätsbibliothek der RWTH Aachen, 2015.
[11] A PCC Company Special Metals, Product handbook of high-performance nickel alloys. The alloy specialists, Available at: https://www.google.de/url?sa=t&rct=j&q=&esrc=s&source=web&cd=1&cad=rja&uact=8&ved=0ahUKEwjI077e24jWAhUBtxQKHWFsBOsQFggtMAA&url=http%3A%2F%2Fwww.specialmetals.com%2Fassets%2Fsmc%2Fdocuments%2Fpcc-8064-sm-alloy-handbook-v04.pdf&usg=AFQjCNHmuBqtyHqJ5hPbnYTnl-VMQ1mkhA.
[12] C. Zhong, et al., A comparative study of Inconel 718 formed by high deposition rate laser metal deposition with GA powder and PREP powder, Mater. Des. 107 (2016) 386–392.
[13] H. Xiao, S. Li, X. Han, J. Mazumder, L. Song, Laves phase control of Inconel 718 alloy using quasi-continuous-wave laser additive manufacturing, Mater. Des. 122 (2017) 330–339.
[14] L.L. Parimi, G.A. Ravi, D. Clark, M.M. Attallah, Microstructural and texture development in direct laser fabricated IN718, Mater. Char. 89 (2014) 102–111.
[15] C.H. Radhakrishna, K.P. Rao, The formation and control of Laves phase in superalloy 718 welds, J. Mater. Sci. 32 (1997) 1977–1984.
[16] G.J. Ram, A.V. Reddy, K.P. Rao, G.M. Reddy, J.S. Sundar, Microstructure and tensile properties of Inconel 718 pulsed Nd-YAG laser welds, J. Mater. Process. Technol. 167 (2005) 73–82.
[17] Schirra, J. J., Caless, R. H. & Hatala, R. W. The Effect of Laves Phase on the Mechanical Properties. The Minerals, Metals & Materials Society, 375–388.
[18] G.A. Rao, M. Kumar, M. Srinivas, D.S. Sarma, Effect of standard heat treatment on the microstructure and mechanical properties of hot isostatically pressed superalloy inconel 718, Mater. Sci. Eng., A 355 (2003) 114–125.
[19] M. Sundararaman, P. Mukhopadhyay, S. Banerjee, Some aspects of the precipitation of metastable intermetallic phases in Inconel 718, Metall. Trans. A 23 (1992) 2015–2028.
[20] H. Qi, M. Azer, A. Ritter, Studies of standard heat treatment effects on microstructure and mechanical properties of laser net shape manufactured Inconel 718, Metall. Mater. Trans. 40 (2009) 2410–2422.
[21] P.L. Blackwell, The mechanical and microstructural characteristics of laser-deposited IN718, J. Mater. Process. Technol. 170 (2005) 240–246.
[22] F. Liu, et al., Microstructure and residual stress of laser rapid formed Inconel 718 nickel-base superalloy, Opt Laser. Technol. 43 (2011) 208–213.
[23] Homogenization and Thermomechanical Processing of Cast Alloy 718, PROCEEDING OF INTERNATIONAL SYMPOSIUM ON SUPERALLOYS, 1991.